AGU PUBLICATIONS

Water Resources Research

RESEARCH ARTICLE
10.1002/2015WR017325

Key Points:
- ^{129}I fallout was measured in Vancouver after the Fukushima-Daiichi nuclear accident
- A ^{129}I pulse was identified in precipitation and potentially in local groundwater
- Vadose zone modeling constrained adsorption and transport of ^{129}I into groundwater

Supporting Information:
- Supporting Information S1
- Table S1
- Table S2
- Table S3
- Table S4

Correspondence to:
M. N. Herod,
mattherod@gmail.com

Citation:
Herod, M. N., M. Suchy, R. Jack Cornett, W. E. Kieser, I. D. Clark, and G. Graham (2015), The atmospheric transport of iodine-129 from Fukushima to British Columbia, Canada and its deposition and transport into groundwater, *Water Resour. Res.*, *51*, 9628–9645, doi:10.1002/2015WR017325.

Received 31 MAR 2015
Accepted 7 NOV 2015
Accepted article online 12 NOV 2015
Published online 17 DEC 2015

The atmospheric transport of iodine-129 from Fukushima to British Columbia, Canada and its deposition and transport into groundwater

Matt N. Herod[1], Martin Suchy[2], R. Jack Cornett[1], W. E. Kieser[1], Ian D. Clark[1], and Gwyn Graham[2]

[1]André E. Lalonde Accelerator Mass Spectrometry Lab, Department of Earth Science, University of Ottawa, Ottawa, Ontario, Canada, [2]Environment Canada, Transboundary Water Management, Vancouver, British Columbia, Canada

Abstract The Fukushima-Daiichi nuclear accident (FDNA) released iodine-129 (15.7 million year half-life) and other fission product radionuclides into the environment in the spring and summer of 2011. ^{129}I is recognized as a useful tracer for the short-lived radiohazard ^{131}I, which has a mobile geochemical behavior with potential to contaminate water resources. To trace ^{129}I released by the FDNA reaching Canada, pre-accident and post-accident rain samples collected in Vancouver, on Saturna Island and from the National Atmospheric Deposition Program in Washington State were measured. Groundwater from the Abbotsford-Sumas Aquifer was sampled to determine the fate of ^{129}I that infiltrates below the root zone. Modeling of vadose zone transport was performed to constrain the travel time and retardation of ^{129}I. The mean pre-accident ^{129}I concentration in rain was 31×10^6 atoms/L (n = 4). Immediately following the FDNA, ^{129}I values increased to 211×10^6 atoms/L and quickly returned to near-background levels. However, pulses of elevated ^{129}I continued for several months. The increases in ^{129}I concentrations from both Vancouver and Saturna Island were synchronized, and occurred directly after the initial release from the FDNA. The ^{129}I in shallow (^{3}H/^{3}He age <1.4 years) Wassenaar et al. (2006) groundwater showed measurable variability through March 2013 with an average of 3.2×10^6 atoms/L (n = 32) that was coincident with modeled travel times for Fukushima ^{129}I. The groundwater response and the modeling results suggest that ^{129}I was partially attenuated in soil, which is consistent with its geochemical behavior; however, we conclude that the measured variability may be due to Fukushima ^{129}I entering groundwater.

1. Introduction

On 11 March 2011, a magnitude 9.0 earthquake occurred near Tōhoku, Japan, causing a tsunami that damaged the Fukushima-Daiichi Nuclear Power Plant (FDNPP) and released radionuclides to the ocean and atmosphere. The primary radionuclides released were ^{131}I (half-life: 8 days), ^{134}Cs (half-life: 2 years) and ^{137}Cs (half-life: 30 years). However, numerous other fissionogenic isotopes were also released and are measurable in the environment including iodine-129 (half-life: 15.7×10^6 years) [*Steinhauser*, 2014]. The total quantity of ^{131}I released to the atmosphere has been estimated between 120 and 200 PBq and using this number the quantity of ^{129}I can be calculated from the ^{129}I/^{131}I fissionogenic ratio, which was estimated to be 31.6 [*Miyake et al.*, 2012]. This calculation yields a range of atmospheric ^{129}I released from 0.81 to 1.4 kg [*Tokyo Electric Power Company*, 2012]. This quantity, while significant, is far less than the annual gaseous releases from nuclear fuel reprocessing, which have been estimated at 6–12 kg/yr [*Moran et al.*, 1999]. However, the nature of the releases from the Fukushima-Daiichi Nuclear accident (FDNA), which were isolated in time and space, provide a rare opportunity to study the transport of ^{129}I and its environmental cycling and distinguish them from other releases of ^{129}I from nuclear fuel reprocessing and past bomb testing.

Radionuclides released from the FDNA have been detected across the globe [*Bikit et al.*, 2012; *Evrard et al.*, 2012; *Landis et al.*, 2012; *Macmullin et al.*, 2012; *Melgunov et al.*, 2012; *Piñero García and Ferro García*, 2012; *Wetherbee et al.*, 2012]. These radionuclides were transported primarily in the atmosphere and deposited by both dry deposition and washout [*Wetherbee et al.*, 2012]. Atmospheric transport and deposition via precipitation of ^{129}I has been well studied in the context of releases from nuclear fuel reprocessing sites such as La Hague and Sellafield, and Paul et al. investigated the dispersion and wet deposition of

^{129}I from the Chernobyl accident [*Paul et al*., 1987; *Persson et al*., 2007; *Aldahan et al*., 2009]. Iodine has been shown to have an atmospheric residence time of 10–14 days, which allows releases of ^{129}I and ^{131}I to travel great distances from their point source [*Jabbar et al*., 2013]. It has been assumed that the fate of ^{129}I deposited on the ground surface is to mix and distribute throughout the environment and a large amount of research has focused on the terrestrial cycling of iodine in surficial environments such as soil, rivers, and plants [*Bamba et al*., 2014; *Muramatsu et al*., 2015]. However, a few studies have investigated the infiltration of ^{129}I into groundwater. Modern recharge waters in the nearby Milk River Aquifer, Alberta, showed meteoric values for ^{129}I concentration and the ^{129}I/^{127}I ratio of 8.6×10^5 atoms/L and 1.1×10^{-11}, respectively [*Fabryka-Martin et al*., 1991]. Young groundwater from the Orange County Aquifer in southern California had ^{129}I concentrations that ranged from 12–53 $\times 10^6$ atoms/L and ^{129}I/^{127}I ratios of 0.9 to 4.5 $\times 10^{-10}$ in samples with groundwater ages of less than 2 years [*Schwehr et al*., 2005].

^{129}I has shown promise as a conservative, long lived, tracer of groundwater [*Schwehr et al*., 2005], although its attenuation during recharge through the soil must be considered. A wide variety of K_d values for iodine have been measured in many different soil types and due to the biophilic nature of iodine, soils that have high organic matter content tend to be very efficient at adsorbing iodine at ambient concentrations with K_d values as high 1800 L/kg in peat [*Sheppard et al*., 1996; *Zhang et al*., 2011]. However, in soils with low organic matter iodine has been observed to behave semi-conservatively and have K_d values as low as 0.1 L/kg in the I^- state [*Alvarado-Quiroz et al*., 2002; *Schwehr et al*., 2005]. Typically, K_d values for iodine fall in the range of 0.2–35 L/kg for sandy soils [*Söderlund et al*., 2011]. Iodide, I^-, has lower K_d values than the iodate IO_3^- [*Fukui et al*., 1996] and the K_d decreases for both iodide and iodate at neutral to alkaline pH [*Fukui et al*., 1996]. Studies of ^{129}I migration and retardation in groundwater have been conducted at the ^{129}I contaminated Hanford and Savannah River nuclear sites. These nuclear fuel reprocessing plants, which are now closed, were point sources of ^{129}I in the region in the past. Results have shown that the mobility of ^{129}I contamination in the subsurface is dependent on the iodine concentration, with high concentrations having lower K_d's as well as other factors such as organic content, speciation and pH. The most important of these is the organic content [*Hu et al*., 2005, 2012; *Zhang et al*., 2011]. Studies of groundwater from the Idaho Falls nuclear site have also shown that ^{129}I can be transported vertically and laterally great distances within the aquifer. However, dilution and dispersion have reduced ^{129}I contamination as further inputs have ceased [*Bartholomay*, 2013].

The objective of this study was to trace the fate of the FDNA ^{129}I release through precipitation and groundwater recharge in a well-characterized sandy aquifer on the west coast of Canada. Archived pre-FDNA precipitation samples were obtained and weekly precipitation samples were collected for 1 year immediately following the FDNA. We then investigated the fate of the ^{129}I deposited and its attenuation during infiltration into the shallow, sandy aquifer. Sampling of two different well sites with different recharge times was conducted on a monthly to bi-monthly basis over the course of a year. The recharge time of the wells was established by ^{3}H/^{3}He dating to be 11 and 14 months, respectively. This aspect of the work simulates an aquifer scale tracer experiment and provides insight into the long term environmental behavior of ^{129}I in the hydrosphere and contaminant travel times in the vadose zone of the aquifer.

1.1. Hydrogeology of the Abbotsford-Sumas Aquifer

The Abbotsford-Sumas Aquifer (ASA) is an extensive unconfined aquifer with a surficial area of ~200 km^2. It spans the Canada–U.S. border between southern British Columbia, Canada, and Washington State, USA and supplies ~120,000 people with drinking water (Figure 1). The hydraulic properties of the ASA have been studied in the context of nitrate leaching and transport as the primary land use in the region is agriculture with a high density of berry farming (raspberries and blueberries), poultry production and some dairy farms [*Wassenaar*, 1995; *Cox and Kahle*, 1999; *Wassenaar et al*., 2006; *Chesnaux et al*., 2007]. NO_3 contamination throughout much of the aquifer is attributed to the intensive nature of agricultural activities in this area [*Hii et al*., 1999; *Chesnaux and Allen*, 2007; *Zebarth et al*., 2015].

Both wells sampled are completed in the upper 20 m of an unconsolidated gravel and coarse sand aquifer with discontinuous lenses of till and clay which continues to a depth of up to 60 m, underlain by a glaciomarine clay aquitard [*Cox and Kahle*, 1999; *Graham et al*., 2014]. The heterogeneous

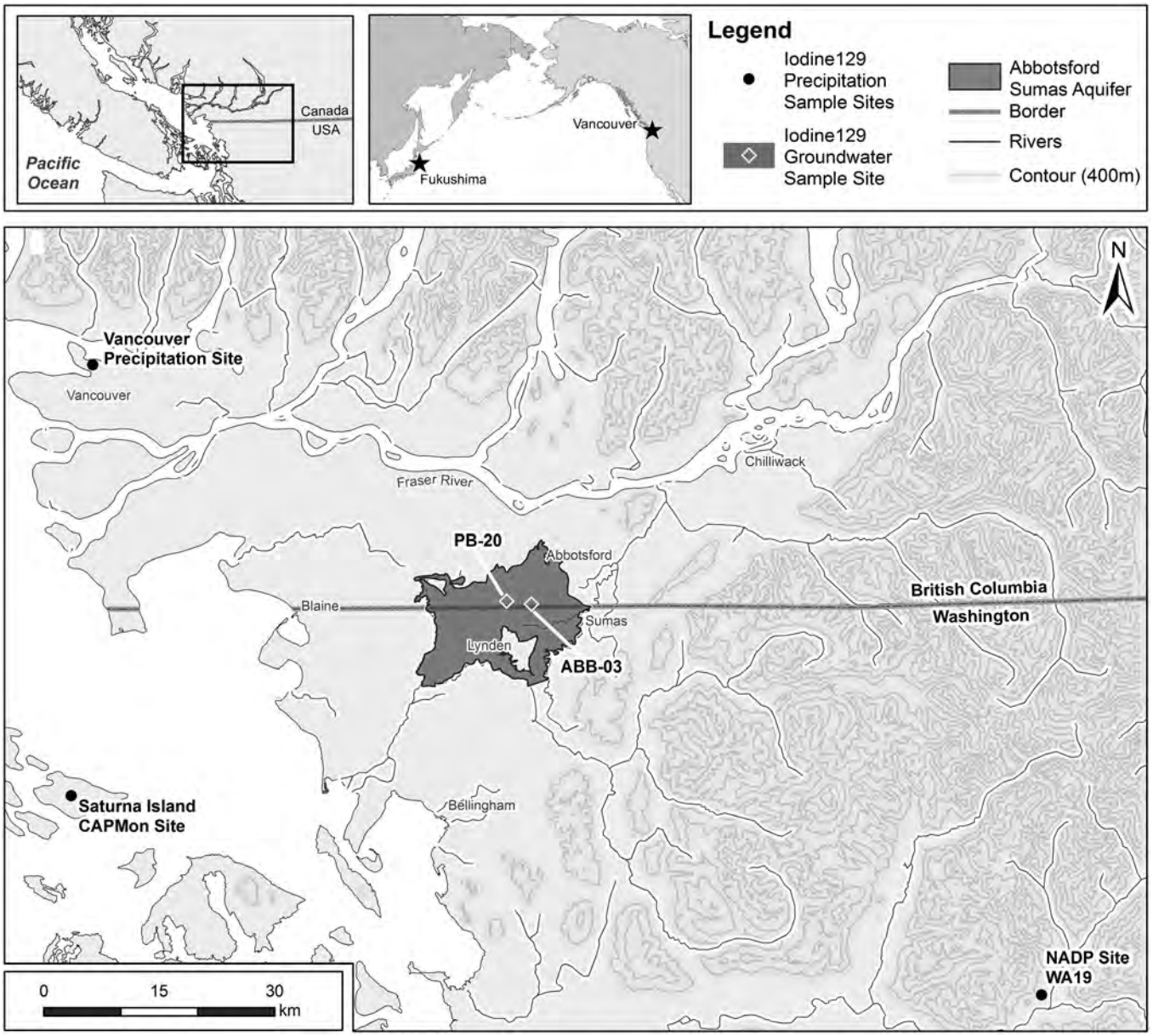

Figure 1. Sample map showing location of all three precipitation sampling locations as well as the location of both wells used for groundwater sampling. The surface expression of the Abbotsford-Sumas Aquifer is shaded.

stratigraphy has produced complex, preferential flow paths, which can result in rapid transport of water and contaminants through the vadose zone (supporting information Figure S1) [*Scibek and Allen*, 2006]. Hydraulic conductivities in the saturated zone range from 2 to 2400 m/d with a median of 82 m/d [*Cox and Kahle*, 1999]. Groundwater flow is subradial with near-vertical recharge and a strong linear relationship between depth and groundwater age [*Wassenaar et al*., 2006; *Chesnaux et al*., 2012].

Recharge in the ASA has been estimated at between 650 and 1150 mm/yr [*Scibek and Allen*, 2006], representing up to 60–80% of the annual average precipitation which is 1500 mm/yr [*Chesnaux and Allen*, 2007]. On a seasonal basis the water table can range as much as 4 m/yr in some wells [*Hii et al*., 1999]. Precipitation and recharge are maximized in the fall and winter leading to the highest water level at this point of the year, although there is often a delay of 1–3 months between peak precipitation and water level response [*Wassenaar et al*., 2006; *Chesnaux and Allen*, 2007; *Graham et al*., 2014].

2. Methods

2.1. Sampling Sites

2.1.1. Precipitation Sampling

Rooftop precipitation samples were collected from a federal building located in downtown Vancouver, BC between 18 March 2011 and 8 March 2012 (Figure 1). Precipitation was collected using an 8 in. nonrecording Stand Rain Gauge. The Rain Gauge funnel and sample collection bag was fixed onto a white 20 L bucket and lid. Water was collected on an approximately weekly basis, and transferred to certified trace clean 250 mL Nalgene® bottles, then frozen prior to shipment. Precipitation samples were also donated by National Atmospheric Deposition Program (NADP) in the United States from site WA19 in northern Washington State. These samples consisted of ~30 mL weekly samples. Four samples were then composited to represent monthly sampling intervals for pre-Fukushima. Several pre-Fukushima and post-Fukushima accident samples were also donated by the Canadian Air and Precipitation Monitoring Network (CAPMoN) from nearby Saturna Island (Figure 1).

2.1.2. Groundwater Sampling

Groundwater samples were collected from two dedicated Environment Canada monitoring piezometers (PB20 and ABB03) with a $^{3}H/^{3}He$ groundwater age of less than 2 years [*Wassenaar*, 1995; *Wassenaar et al*., 2006]. The average historical (1989-present) groundwater depth at site PB20 is 3.3 m below ground surface (mbgs), while the midscreen depth is 3.9 mbgs, resulting in a shallow average pressure head of <1 m. For ABB03, the average water level depth (1988-present) is 11.5 mbgs, and a midscreen piezometer depth of 17.1 mbgs, resulting in an average pressure head of <6 m.

The lithology of the two wells sampled is very similar. Both are primarily composed of coarse grained sand and gravel beds that range from well to poorly sorted with numerous cobbles of greater than 5 cm. There are also occurrences of sand lenses and interbedded layers of sand and gravel (supporting information Table S1).

Samples were collected using a Grundfoss® stainless steel submersible pump, Teflon® lined LDPE tubing, and stainless-steel fittings and valves. The water was pumped directly through a flow-through cell housing a YSI® multiprobe sonde (temperature, pH, electrical conductivity, redox potential, and dissolved oxygen). Samples were collected after at least three casing volumes were removed from the wells and the YSI® field parameters had stabilized. All bottles were rinsed with sample water prior to filling and filled into 1 L LDPE bottles, stored at 5°C for archiving.

2.2. Preparation of Samples for ^{129}I Analysis

Iodine was extracted from samples of precipitation and groundwater using the silver iodide precipitation method with stable ^{127}I carrier ($^{129}I/^{127}I$: $15.6 \pm 0.6 \times 10^{-14}$) as described in *Sheppard and Herod* [2012] and *Herod et al*. [2013]. ^{129}I in the AgI targets was measured using the University of Ottawa's IsoTrace Accelerator Mass Spectrometer. ^{127}I was measured in all samples using an Agilent 7700 Inductively Coupled Plasma Mass Spectrometer at the University of Ottawa.

2.3. Vadose Zone Recharge and Transport Modeling

The infiltration of atmospheric ^{129}I from the FDNA and natural ^{127}I through the vadose zone of the Abbotsford-Sumas Aquifer was modeled using the USGS software VS2DTI, which simulates water and contaminant transport through variably saturated porous media and yields numerical results for a variety of fluid and mass balance parameters [*Lapala et al*., 1987; *Healy*, 1990]. The model incorporates soil and hydraulic properties representative of the region. A transient simulation was performed using the weekly input of rain and iodine and a basic water balance approach was used. Infiltration and ^{129}I concentration were adjusted for evapotranspiration [*Farmwest*, 1998; *Chesnaux and Allen*, 2007], which exceeds precipitation between May and September leading to a substantial moisture deficit in the soil and necessitates irrigation. Four mm/d (T. VanDer Gulik, personal communication, 2014) of irrigation water with the median ^{129}I for the ASA groundwater was included in the model to simulate the actual mass flux of ^{129}I entering the aquifer during periods with negligible precipitation as local groundwater is used for irrigation. This represents 484 mm of water added between 14 May 2011 and 14 September 2011 and an additional ^{129}I mass flux of 11.2×10^{6} atoms/m^2/d during relevant periods.

The Van Genuchten equation was employed to describe the hydraulic conductivity of the vadose zone from the input parameter of saturated hydraulic conductivity [*van Genuchten*, 1980]. Model input data for the vadose zone soil used a combination of default values for medium sand and measured values for the ASA. The input data are provided in supporting information Table S2. Porosity, hydraulic conductivity, residual moisture content were obtained from literature and K_d was calculated [*Chesnaux and Allen*, 2007; *Chesnaux et al*., 2007]. All other hydraulic parameters were default values. Longitudinal and transverse dispersion were set at one half of the maximum grid spacing, which in this case was 0.7 and 0.015, respectively. Varying the thickness of the vadose zone did not affect transport times in the model due to the conductive nature of the soils. In this model, a range of K_d values was used with a linear isotherm to consider the adsorption of iodine in the ASA soils [*Sheppard et al*., 1996].

Boundary conditions that were applied to the model consisted of a recharge flux corresponding to the precipitation the Abbotsford region received during each of the 42 recharge periods. Each recharge period was defined as the interval used in precipitation sampling. The water table was used as the lower boundary condition of the model and was set using an equilibrium profile in which the water table had a pressure head of 0. A measured concentration of ^{129}I in precipitation was applied to each recharge period and an initial concentration of 2.4×10^6 atoms/L was used within the vadose zone.

3. Results and Discussion

3.1. Precipitation

3.1.1. ^{129}I, ^{127}I, and ^{129}I/^{127}I in Precipitation

The ^{127}I concentration in precipitation (Table 1 and Figure 2; precipitation data in supporting information Table S3) ranged between 2.8 and 9.2 μg/L with an average of 4.3 and a median of 4.1 ppb (n = 51). This range agrees well with the range reported in the literature for North America and Europe (0.2–12 μg/L) [*Moran et al*., 1999; *Gómez-Guzmán et al*., 2012] although the average value reported here is approximately 1–2 μg/L higher than the average value observed by others, likely due to the proximity of this study to the ocean, which provides a vapor source enriched in ^{127}I to local precipitation [*Fuge and Johnson*, 1986; *Persson et al*., 2007]. It has also been proposed that orographic lifting of air masses can lead to a depletion of iodine irrespective of distance from the coast [*Reithmeier et al*., 2006; *Gilfedder et al*., 2007].

The pre-FDNA ^{129}I values that were measured in precipitation from three NADP composite samples and one Saturna Island sample ranged from 13–53 $\times 10^6$ atoms/L with a mean of 31 $\times 10^6$ atoms/L and a median of 28 $\times 10^6$ atoms/L (n = 4; Table 1 and Figure 2). This agrees well with other ^{129}I concentrations measured in precipitation in the south and central regions of the US, which show a ^{129}I concentration range of 7–60 $\times 10^6$ atoms/L and an average of 27 $\times 10^6$ atoms/L (n = 13) [*Moran et al*., 1999]. Past operation of the Hanford nuclear fuel reprocessing facility in Washington State resulted in locally higher atmospheric ^{129}I with precipitation in 1973 reaching 6.8×10^{11} atoms/L [*Brauer and Rieck*, 1973; *Moran et al*., 1999]. The Hanford facility was shut down in 1972 and our measurements suggest that it is no longer a significant source of ^{129}I to the atmosphere [*Aldahan et al*., 2007].

A pulse of ^{129}I in precipitation with maximum concentrations of 211 $\times 10^6$ atoms/L in Vancouver and 221 $\times 10^6$ atoms/L at Saturna Island was observed 6 days following the FDNA. A value of 311 $\times 10^6$ atoms/L was also measured during the first week of July 2011 in Vancouver precipitation, well after atmospheric releases from FDNPP had ceased. The samples from all three sites have a post-accident mean of $70 \pm 60 \times 10^6$ atoms/L (n = 45), which is over twice the pre-accident average of $31 \times 10^6 \pm 17$ atoms/L (n = 4) and previous measurements of ^{129}I in precipitation elsewhere in North America in recent years [*Moran et al*., 1999]. The overlap between these means when 1σ is considered is due to the length of sampling period and the variability of ^{129}I concentrations. These concentrations are considerably lower than the 76×10^{10} atoms/L measured in precipitation at Fukushima following the FDNA [*Xu et al*., 2013].

In pre-FDNA samples the ^{129}I/^{127}I ratio ranged from 0.7 to 4.0×10^{-9} and immediately following the release of radionuclides from the FDNPP the ^{129}I/^{127}I ratio increased 6–10 times above background at all three sites and reached a high of nearly 11×10^{-9} at the Vancouver site (Figure 2). This demonstrates that the increases in ^{129}I were not accompanied by corresponding increases in stable I, which was constant, but rather inputs of ^{129}I from a radioiodine source.

Table 1. Summary of Key Statistics for the Precipitation Data Set for ^{129}I, ^{127}I, and $^{129}I/^{127}I$

	Precipitation Key Stats								
Site	^{129}I Range	^{129}I Median	^{129}I Mean	^{127}I Range	^{127}I Median	^{127}I Mean	$^{129}I/^{127}I$ Range (10^{-9})	$^{129}I/^{127}I$ Median (10^{-9})	$^{129}I/^{127}I$ Mean (10^{-9})
Vancouver	10.87–310.74	41.95	61.61	9.18–2.85	4.14	4.26	0.68–13.39	2.34	3.09
Saturna	13.19–220.65	83.99	106.33	5.13–3.12	3.97	4.12	0.7–9.17	5.08	5.09
NADP	25.77–95.42	41.58	51.09	6.04–2.83	4.41	4.42	0.9–6.29	2.54	3.07
All		44.35	67.14		4.13	4.25		2.51	3.38

In order to determine if the FDNA input of ^{129}I had a statistically significant impact on ^{129}I concentrations in rainfall and if background levels were reached later in the year two tailed students *t* tests were performed to determine the relationship between the means of pre-, para-, and post-FDNA sampling intervals. The sampling interval for para-FDNA affected rain ranged from 18 March to 20 May 2011. This interval was determined using publicly accessible Health Canada radionuclide data from the Sidney, BC air filter station [*Health Canada*, 2014]. The results of the *t* tests lead to three conclusions: (1) The mean ^{129}I concentration for post-FDNA rain is significantly greater than the mean for pre-FDNA ^{129}I ($p = 0.01$, $\alpha = 0.05$). (2) The mean ^{129}I concentration for para-FDNA rain is significantly greater than the mean ^{129}I concentration in rain following the FDNA, when the one outlying point in July is omitted ($p = 0.002$, $\alpha = 0.05$). (3) The mean

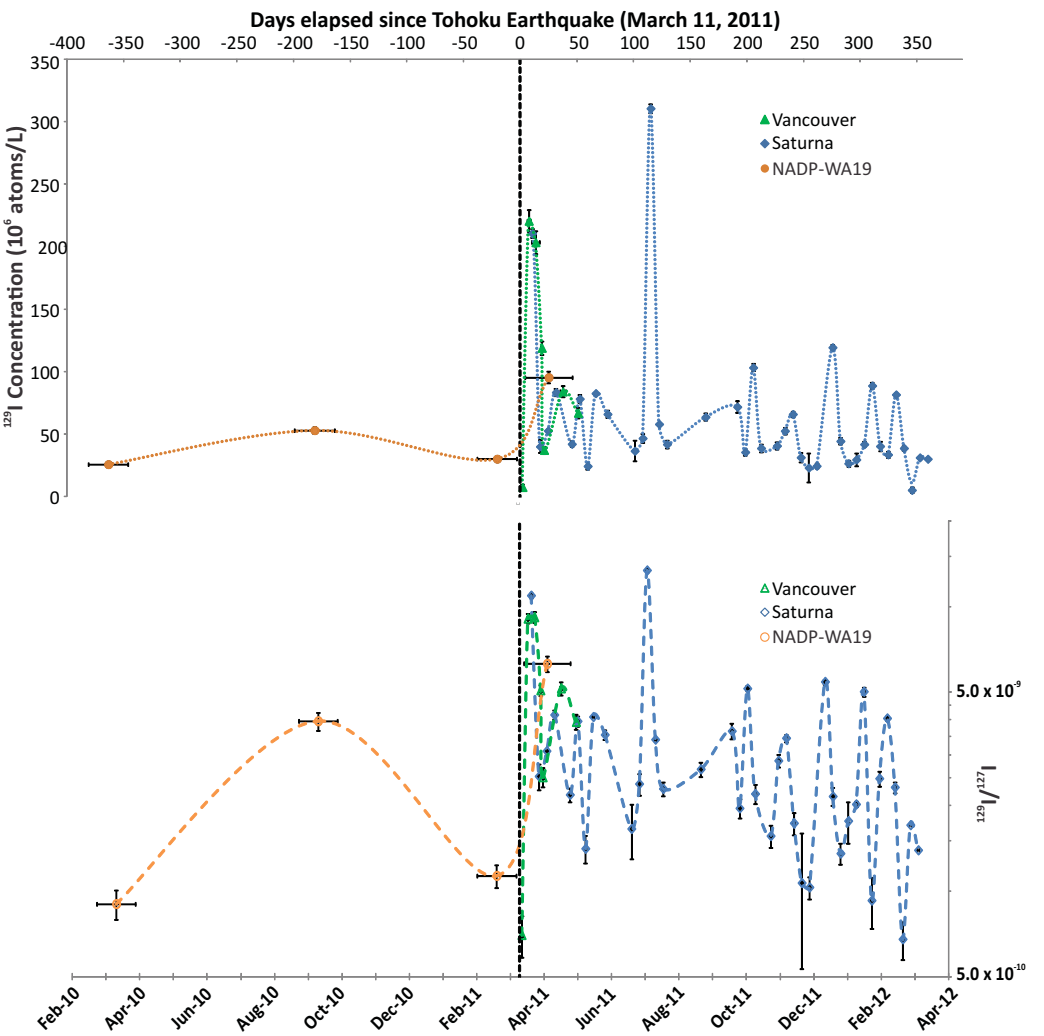

Figure 2. Variation in the concentration of ^{129}I and the $^{129}I/^{127}I$ ratio in precipitation from Vancouver, Saturna Island, and NADP site WA19 over time. The time range that each NADP sample integrates is displayed using horizontal error bars. 1σ error is contained within data points if not visible. The dashed vertical line shows the date of the FDNA relative to samples.

concentration in pre-FDNA rain is not significantly different than the mean for the post-FDNA interval when the one outlying point in July is included ($p = 0.096$, $\alpha = 0.05$). This confirms that following 20 May 2011 the average ^{129}I concentration in rain had returned to pre-FDNA background levels.

3.1.2. Temporal Variation of Atmospheric ^{129}I Concentrations

The high ^{129}I concentrations while the FDNA was ongoing are attributed to the rapid trans-Pacific transport of ^{129}I from Fukushima. This source was confirmed using the NOAA's HYSPLIT back trajectory atmospheric modeling program (supporting information Figure S2) [*Draxler and Rolph*, 2013]. This response in ^{129}I concentrations shows that radionuclides from Fukushima were transported rapidly from Japan to the west coast of Canada and the US and a peak in ^{129}I concentrations could be observed within 6–10 days of the FDNA. This observation agrees well with the findings of other studies that observed an increase in the ^{131}I and ^{137}Cs concentrations in air filters on the west coast of North America by 17 March, and a peak on 19–20 March 2011 [*Leon et al*., 2011; *Wetherbee et al*., 2012]. Furthermore, the NADP sample, which is a composite of rainfall events spanning 15 March 2011 to 16 April 2011 shows a significantly elevated ^{129}I concentration of 95×10^6 atoms/L.

3.1.3. The July Spike in Atmospheric ^{129}I

There was a spike in ^{129}I concentration observed in the precipitation sample from the period of 1 July 2011 to 8 July 2011, over 4 months after the FDNA. For this sample the ^{129}I concentration rose to $311 \pm 8.4 \times 10^6$ atoms/L (duplicate analysis was within 1σ), which is a substantially higher concentration than any other sample measured in this study. As monitoring at Fukushima detected no pulse of ^{129}I in precipitation in July despite the ongoing efforts to stabilize the reactors at the time [*Xu et al*., 2013], this spike is likely due to a punctuated release from a nuclear fuel reprocessing facility. Modeling of the air parcel back trajectories using the NOAA HYSPLIT model for the sampling period shows air mass trajectories from Hawaii, north Japan, and Russia (supporting information Figure S3). Despite its high concentration this spike had a low ^{129}I mass deposition due to the small volume of rain during this period.

3.1.4. Deposition Flux of ^{129}I as Washout

The mass of ^{129}I deposited via precipitation as washout was calculated using the equation [*Baker et al*., 2001]:

$$\psi = (C \times P)/T \tag{1}$$

Here ψ is the washout or mass flux of iodine throughout the sampling period (atoms/m^2/d), C is the concentration of ^{129}I or ^{127}I in the rainwater sample, P is the precipitation at Vancouver Airport (mm), and T is the time interval of the sampling period in days. The results of this calculation are listed in Table 2 and their fluctuation over time is pictured in Figure 3. Washout in samples from Vancouver ranged from 6.6×10^8 atoms/m^2/d, in the first sample following the FDNA, to 3.1×10^7 atoms/m^2/d and the samples from Saturna Island ranged from 2.6×10^9 to 3.7×10^7 atoms/m^2/d. The maximum values for both Saturna Island and Vancouver coincide during the peak concentration of ^{129}I in para-FDNA precipitation.

The principal factor that controls the magnitude of the mass flux is the concentration of ^{129}I. Indeed, the concentration of ^{129}I is significantly correlated to the mass flux with an r of 0.49 ($p = 0.0046$). Precipitation quantity and washout are also correlated with an r of 0.35 ($p = 0.031$). This relationship can clearly be seen in Figure 3, which shows the washout and the precipitation quantity for each sampling interval. The influence of dry deposition has not been considered as most research has suggested that dry deposition plays a less important role in ^{129}I mass flux than wet [*López-Gutiérrez et al*., 2001] particularly given that the Canadian west coast receives ~1500 mm of precipitation annually.

3.2. Groundwater

3.2.1. ^{129}I Concentration and ^{129}I/^{127}I in Groundwater

A time lag of 0.9 ± 0.5 and 1.2 ± 0.5 years, respectively, for monitoring wells ABB03 and PB20 for transport from the water table to the well screen was established using ^{3}H/^{3}He [*Wassenaar et al*., 2006]. The range in ^{129}I concentration for groundwater in the wells ABB03 and PB20 was 0.31 to 9.2×10^6 atoms/L and 0.4 to 6.3×10^6 atoms/L, respectively (Figure 4, Table 3 and supporting information Table S4), with median concentrations of 2.1×10^6 and 3.5×10^6 atoms/L, respectively. Several samples had uncertainties high enough to overlap with the lower limit of detection suggesting current background ^{129}I levels, which are still above the pre-nuclear ^{129}I background, may be even lower than those measured here meaning that detection of the anomalous peaks in ^{129}I concentration are robust as they are well above this limit. The

Table 2. Results of Washout Calculations for Precipitation Samples from Vancouver and Saturna Island[a]

Location	Sample ID	Sampling Start	Sampling End	Precip (L/m^2)	Precip/day ($mm/m^2/d$)	^{129}I Washout ($atoms/m^2/interval$)	^{129}I Washout ($atoms/m^2/d$)
Vancouver							
	VP1	18 Mar 2011	25 Mar 2011	22	3.14	4.63E+09	6.62E+08
	VP2	25 Mar 2011	1 Apr 2011	58	8.29	2.32E+09	3.32E+08
	VP3	1 Apr 2011	8 Apr 2011	34	4.86	1.79E+09	2.56E+08
	VP4	8 Apr 2011	15 Apr 2011	28	4.00	2.33E+09	3.34E+08
	VP7			2			
	VP5	22 Apr 2011	29 Apr 2011	25	3.57	1.05E+09	1.50E+08
	VP8	29 Apr 2011	6 May 2011	11	1.57	8.59E+08	1.23E+08
	VP6	6 May 2011	13 May 2011	37	5.29	8.98E+08	1.29E+08
	VP9	13 May 2011	20 May 2011	11	1.57	9.08E+08	1.30E+08
	VP10	20 May 2011	3 Jun 2011	30	2.14	1.98E+09	1.41E+08
	VP11			2			
	VP12	16 Jun 2011	24 Jun 2011	20	2.50	7.28E+08	9.13E+07
	VP13	24 Jun 2011	30 Jun 2011	4	0.67	1.86E+08	3.11E+07
	VP14	30 Jun 2011	8 Jul 2011	7	0.88	2.17E+09	2.72E+08
	VP40	8 Jul 2011	15 Jul 2011	9	1.29	5.21E+08	7.45E+07
	VP15	15 Jul 2011	22 Jul 2011	18	2.57	7.52E+08	1.08E+08
	VP16			3			
	VP17	18 Aug 2011	25 Aug 2011	20	2.86	1.27E+09	1.82E+08
	VP18	15 Sep 2011	22 Sep 2011	40	5.71	2.87E+09	4.10E+08
	VP35	22 Sep 2011	29 Sep 2011	29	4.14	1.03E+09	1.47E+08
	VP19	29 Sep 2011	6 Oct 2011	14	2.00	1.44E+09	2.07E+08
	VP33	6 Oct 2011	13 Oct 2011	16	2.29	6.18E+08	8.84E+07
	VP38	20 Oct 2011	27 Oct 2011	25	3.57	1.01E+09	1.45E+08
	VP21	27 Oct 2011	3 Nov 2011	22	3.14	1.15E+09	1.65E+08
	VP42	3 Nov 2011	10 Nov 2011	8	1.14	5.27E+08	7.54E+07
	VP22	10 Nov 2011	17 Nov 2011	33	4.71	1.03E+09	1.48E+08
	VP31	17 Nov 2011	24 Nov 2011	52	7.43	1.19E+09	1.71E+08
	VP28	24 Nov 2011	1 Dec 2011	29	4.14	7.08E+08	1.01E+08
	VP23	8 Dec 2011	15 Dec 2011	4	0.57	4.77E+08	6.82E+07
	VP27	15 Dec 2011	22 Dec 2011	14	2.00	6.20E+08	8.87E+07
	VP37	22 Dec 2011	29 Dec 2011	68	9.71	1.79E+09	2.57E+08
	VP34	29 Dec 2011	5 Jan 2012	34	4.86	1.00E+09	1.44E+08
	VP24	5 Jan 2012	12 Jan 2012	12	2.00	5.01E+08	8.36E+07
	VP39	12 Jan 2012	19 Jan 2012	9	9.71	7.98E+08	8.62E+08
	VP29	19 Jan 2012	26 Jan 2012	59	4.86	2.37E+09	1.96E+08
	VP36	26 Jan 2012	2 Feb 2012	33	1.71	1.10E+09	5.75E+07
	VP25	2 Feb 2012	9 Feb 2012	14	1.29	1.14E+09	1.05E+08
	VP32	9 Feb 2012	16 Feb 2012	12	8.43	4.64E+08	3.26E+08
	VP41	16 Feb 2012	23 Feb 2012	79	4.71	8.52E+08	5.13E+07
	VP30	23 Feb 2012	1 Mar 2012	51	2.00	1.59E+09	6.24E+07
	VP 26	1 Mar 2012	8 Mar 2012	16	1.71	4.80E+08	5.16E+07
Saturna Island							
	SAT1	13 Mar 2011	13 Mar 2011	6.4	6.40	8.39E+07	8.44E+07
	SAT2	17 Mar 2011	20 Mar 2011	12.8	4.27	2.82E+09	9.41E+08
	SAT3	21 Mar 2011	28 Mar 2011	17.2	2.46	3.50E+09	5.00E+08
	SAT4	29 Mar 2011	31 Mar 2011	43.6	21.80	5.18E+09	2.59E+09
	SAT5	1 Apr 2011	1 Apr 2011	6.2	6.20	2.30E+08	2.30E+08
	SAT6	15 Apr 2011	20 Apr 2011	2.2	0.44	1.84E+08	3.70E+07
	SAT7	30 Apr 2011	2 May 2011	17	8.50	1.14E+09	5.69E+08

[a]Data are presented as both total per sampling interval and normalized to the number of days in each interval. Precipitation quantities are taken from Environment Canada archives for the Vancouver Airport.

magnitude of the ^{129}I anomaly in PB20 is slightly lower than ABB03 potentially due to greater attenuation or dilution during transport to the screen as the recharge time of PB20 is greater than ABB03. The ^{127}I concentrations ranged from 2.9 to 5.7 ppb in ABB03 and 3.1 to 5.2 ppb in PB20. The medians for ^{127}I are 3.8 ppb in ABB03 and 4.3 ppb in PB20, respectively, which are very similar to those measured in precipitation samples (4.3 ppb).

The concentration of ^{129}I in both wells is up to 20 times lower than that of precipitation, unlike stable iodine which is unchanged from levels in precipitation. This recognizes the importance of iodine sorption in soil and the vadose zone as a key attenuation process. Mixing with groundwater with low ^{129}I can be

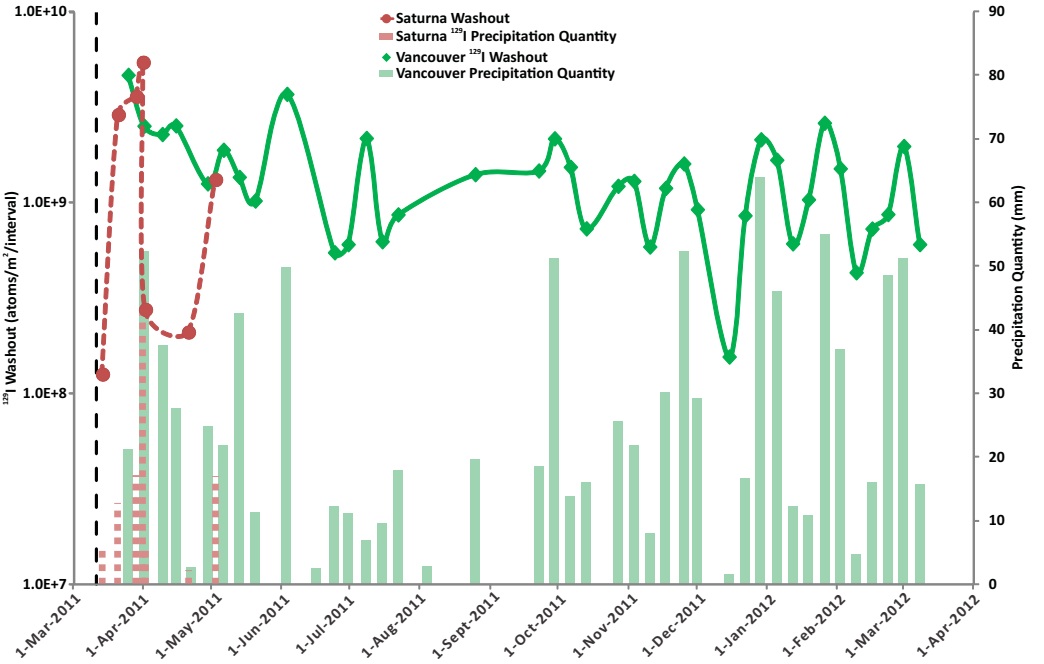

Figure 3. Washout of ^{129}I in Vancouver and Saturna Island. Washout is shown as a line graph on a logarithmic scale on the left. Precipitation quantity is also shown on a linear scale as a bar graph and uses the secondary *y* axis.

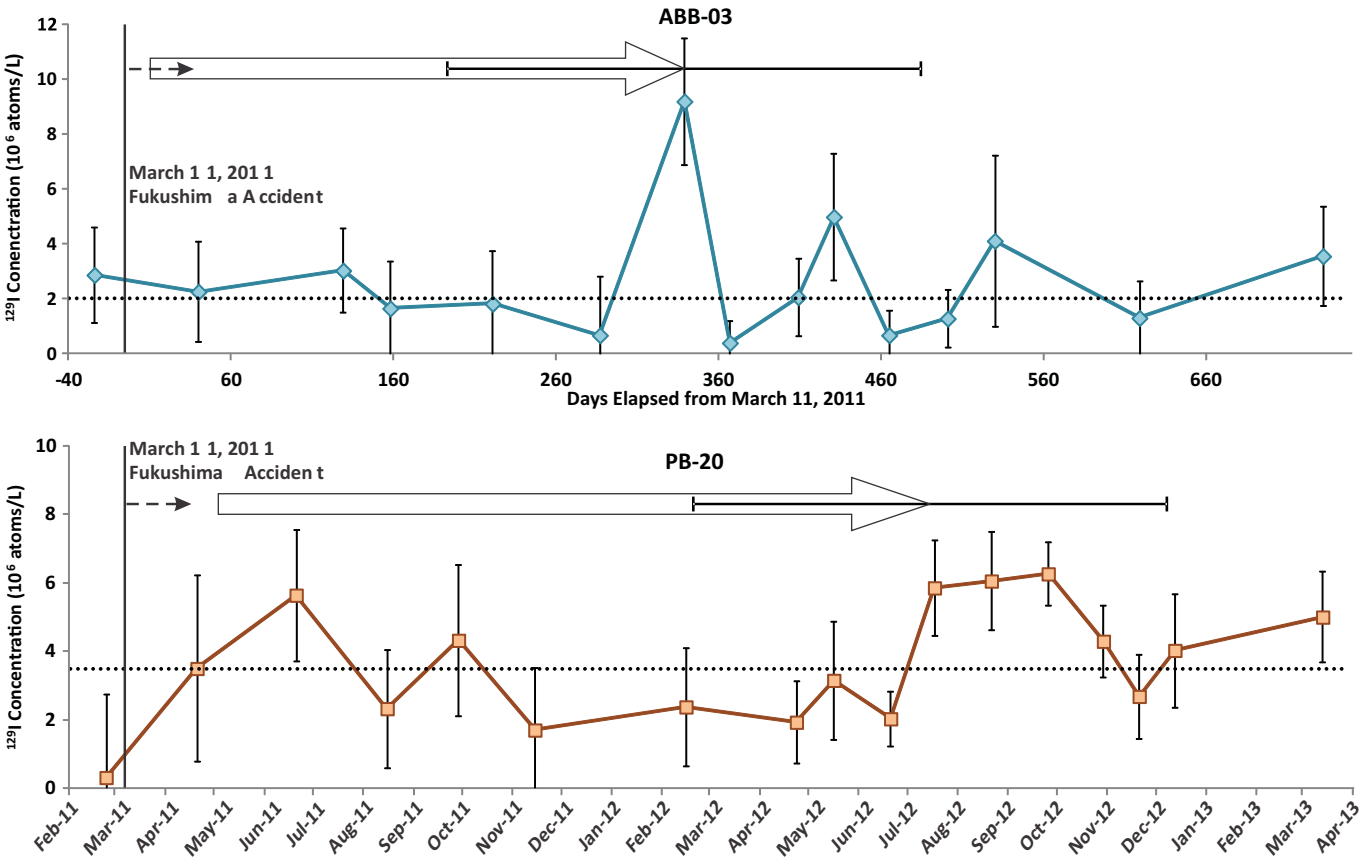

Figure 4. Temporal variation in the concentration of ^{129}I in groundwater in ABB03 and PB20. The solid vertical line shows the date of the Fukushima accident and the dashed horizontal line shows the median of each data set, respectively. The ^{3}H/^{3}He ages from *Wassenaar et al*. [2006] of groundwater in each well and their uncertainty is pictured as the solid arrow which is aligned with the ^{129}I anomaly possibly caused by the FDNA. The dashed arrow covers a 40 day (0.11 year) time span and represents a possible vadose zone transport time.

Table 3. Summary of Key Statistics for Groundwater Data Set Including ^{129}I, ^{127}I, and $^{129}I/^{127}I$

	Groundwater Key Stats								
Well	^{129}I Range	^{129}I Median	^{129}I Mean	^{127}I Range	^{127}I Median	^{127}I Mean	$^{129}I/^{127}I$ Range (x 10^{-11})	$^{129}I/^{127}I$ Median	$^{129}I/^{127}I$ Mean
PB20	0.31–6.27	3.50	3.62	3.11–5.24	4.3	4.17	2.07–37.7	1.70E-10	1.88E-10
ABB03	0.40–9.21	2.07	2.67	2.94–5.7	3.8	3.78	1.87–34.1	1.29E-10	1.48E-10

discounted as nitrate data show that dilution is insufficient in the shallow groundwater to reduce nitrate additions to background [*Wassenaar*, 1995; *Mitchell et al*., 2003; *Wassenaar et al*., 2006]. Nitrate measurements also constrain vadose zone transport times for other conservative tracers. Land use changes or applications of manure to the ground surface can induce a nitrate response in the aquifer within a few months showing that transmission from the ground surface to water table is rapid (Environment Canada, unpublished nitrate data, 2015) (supporting information Figure S4). Previous studies have also shown that spring precipitation can leach nitrate and transport it to the water table in a matter of months [*Wassenaar et al*., 2006; *Chesnaux and Allen*, 2007].

The $^{129}I/^{127}I$ ratios range from 1.9 to 34 $\times$ 10^{-11} for ABB03 and 2.1 to 38 $\times$ 10^{-11} in PB20, and follow variations in the groundwater concentration of ^{129}I very closely due to the low variability for stable I. The *r*-values for both wells show significant correlation coefficients of 0.91 for ABB03 and 0.92 for PB20 ($\alpha = 0.05$) (supporting information Figure S5). The median for ABB03 was 13 $\times$ 10^{-11} and for PB20 it was 17 $\times$ 10^{-11}. These values are one to two orders of magnitude lower than the $^{129}I/^{127}I$ ratios measured in precipitation. This suggests that ^{127}I is not accumulating in the ASA soils whereas there is preferential adsorption of ^{129}I as the aquifer soils equilibrate to the addition of anthropogenic ^{129}I from the nuclear age [*Xu et al*., 2011].

3.2.2. Vadose Zone Transport, K_d, and Retardation of Iodine in the ASA

Retention of ^{129}I from the FDNA on organic matter during recharge through the vadose zone is affected by both organic content of these glacial outwash sediments and the redox state of iodine. The organic matter content in ASA surface soils is low, in the range of 3–9% [*Cox and Kahle*, 1999]. This study measured the dissolved organic carbon (DOC) content in ASA waters and found a mean of 0.45 ppm. Previous work found a median DOC of 0.7 ppm in the Sumas aquifer groundwater [*Cox and Kahle*, 1999; *Chesnaux and Allen*, 2007]. The soil-water partitioning coefficient, K_d, is higher for IO_3^- and organic iodine molecules than for I^- [*Sheppard et al*., 1995; *Fukui et al*., 1996]. Measurements of pH (6.2 $\pm$ 2.2, $n = 61$) and redox (Eh = 618 $\pm$ 67 mV, $n = 61$), in both ASA wells suggest that iodine in the groundwater system is dominantly in the I^-, I_2, or organic iodine state, as it is in precipitation [*Gilfedder et al*., 2008; *Hou et al*., 2009; *Lehto et al*., 2012]. Although, in precipitation ^{129}I, particularly from NFRP's and Chernobyl, has been found to occur 60–80% organic iodine [*Hou et al*., 2009]. Species interconversion can also occur on soils, particularly in the presence of organic carbon [*Hu et al*., 2012]. The soil water partition coefficient, K_d, for the attenuation of ^{129}I and ^{127}I during transport through the vadose zone for precipitation to groundwater can be calculated as [*Schwehr et al*., 2009]:

$$K_d = \frac{V_L \times (C_i - C_f)}{M_S \times C_f} \quad (2)$$

in which V_L is the volume of the aqueous phase (assumed to be 1 L in our calculations), C_i is the initial ^{129}I concentration in the aqueous phase (precipitation), C_f is the ^{129}I concentration in the aqueous phase after equilibration with the vadose zone/aquifer soils (groundwater), and M_s is the mass of the solid phase (assumed to be 1 kg in our calculations). Applying this equation to the median values of data presented in supporting information Tables S2 and S3 K_d values can be produced for both wells. In the case of ABB03, the K_d value was 19 L/kg and in PB20, it was 11 L/kg. These values compare well to those presented in other studies for similar soil types which typically range from 0.2 to 35 or greater [*Muramatsu et al*., 1990; *Alvarado-Quiroz et al*., 2002; *Söderlund et al*., 2011].

In the case of ^{127}I the K_d value, using the median ^{127}I concentration in precipitation as C_i and in groundwater as C_f, for both wells was 0.07 L/kg which is at the very low range for reported K_d values [*Schwehr et al*., 2005]. This exceptionally low K_d for ^{127}I suggests that these soils have equilibrated during Holocene time with the input of stable I from precipitation, potentially limiting soil adsorption capacities for both ^{129}I

and ^{127}I. Attenuation of ^{129}I in the vadose zone is then due to gradual exchange with this reservoir of previously adsorbed stable I on available binding sites either through iodination of organic compounds, anion exchange or adsorption to charged mineral surfaces [*Zhang et al*., 2011]. This suggests that once iodine equilibrium is achieved the transport of iodine to groundwater is conservative. This observation is corroborated by the study of iodine and ^{129}I transport in the Orange County Aquifer, which also found that ^{127}I concentrations remained constant between recharge and groundwater while ^{129}I was strongly attenuated by adsorption [*Schwehr et al*., 2005]. The transport and retardation of ^{129}I in the vadose zone can be explored further using a transient vadose zone model that incorporates the actual quantity and ^{129}I concentration of recharge over time as well as the soil characteristics such as K_d.

3.2.3. Case I: 0 K_d, Homogeneous Sandy Soil, Mean K

Figure 5 shows the evolution of the ^{129}I concentration over time in a hypothetical homogeneous, sandy soil column over the precipitation sampling period. The figure also shows the change in ^{129}I concentration at the water table over the course of the simulation and the change in % saturation over time. In this case a mean K for the sand and gravel soils of the ASA of 138 m/d was used, which was found to represent a mean saturated hydraulic conductivity for the ASA soil based on grain size analysis [*Chesnaux and Allen*, 2007]. The porosity was set to 0.38, which is a representative value for sandy soils [*Freeze and Cherry*, 1979]. The low fluid error (0.01%) and solute mass balance error (−2.6%) suggest model validity for both water and ^{129}I transport over time.

Figure 5a shows the change in % saturation during the simulation. The figure shows the water table located at 7 m depth with a capillary fringe of ∼0.5 m. The saturation is initially at 75% in the soil column; however, as soon as the simulation starts the saturation drops to ∼15–18% and remains in this range for the duration of the simulation. This is indicative of a soil that has a very low field capacity and this scenario agrees well with previous efforts to model the vadose zone of the ASA [*Chesnaux and Allen*, 2007; *Chesnaux et al*., 2007]. This rapid drainage of the vadose zone has a great effect on the mobility and velocity of ^{129}I. The drying of the vadose zone results in a much lower effective hydraulic conductivity in the unsaturated zone and hence greater retardation which inhibits the transport of contaminants, including ^{129}I [*Chesnaux and Allen*, 2007]. Only, subsequent additions of water via precipitation or irrigation can push the ^{129}I front downward toward the water table. This also has an impact on the timing of ^{129}I breakthrough to the water table and smoothing of the ^{129}I concentration profile over time as this phenomenon results in the mixing of water parcels as the ^{129}I proceeds through the vadose zone resulting in a decrease in the peak ^{129}I concentration. This also has the important effect of delaying the transport of the ^{129}I peak to the water table.

Figure 5b shows the depth profile of ^{129}I concentration over time through the vadose zone from the soil surface to its eventual input into groundwater at the base of the profile. Notable is that the flux of ^{129}I is greatest in the first few recharge periods, which were the ones most affected by the FDNA, and had the highest washout values. Following the first few recharge periods the flux of ^{129}I decreases and is variable throughout the rest of the simulation responding to variation in ^{129}I washout and additional inputs from irrigation. The modeled ^{129}I profile within the soil column is also extremely variable due to the fact that there is 0 K_d, which is allowing ^{129}I to infiltrate through the vadose zone nearly unretarded so that the variation in input is partially conserved throughout the depth profile.

Figure 5c shows that the modeled ^{129}I concentration at the water table in this case with no retardation is far higher than the measured ^{129}I concentration groundwater. Notably, the dominantly advective transport in this aquifer could preserve the modeled variability at the water table in groundwater samples.

The timing of the initial increase in ^{129}I concentration at the water table in the model was at ∼40 days and the peak was at ∼259 days (Figure 5b). These values can be used to calculate a ^{129}I transport velocity in a 0 K_d flow path given that we know the distance traveled and the time. Using the initial increase to calculate the ^{129}I velocity yields a mean of 0.18 m/d, whereas using the peak at 259 days gives a velocity of 0.03 m/d. This discrepancy is due to the smoothing and delaying of the peak due to dispersion, sorption and the desaturation of the soil and the rapid drainage the model experienced, which increases retardation greatly. The more reasonable ^{129}I velocity is that calculated by the initial increase at the base of the model as it best represents unimpeded transport of ^{129}I in the 0 K_d system and the peak transport velocity in a preferential flow path.

This profile can be considered an end member for preferential flow in a coarse grained, subvertical bed with 0 K_d. The concentrations that it produces are far higher than those actually measured in ABB03 or PB20, however, the variability in the model groundwater ^{129}I concentrations suggests that a 0 K_d system

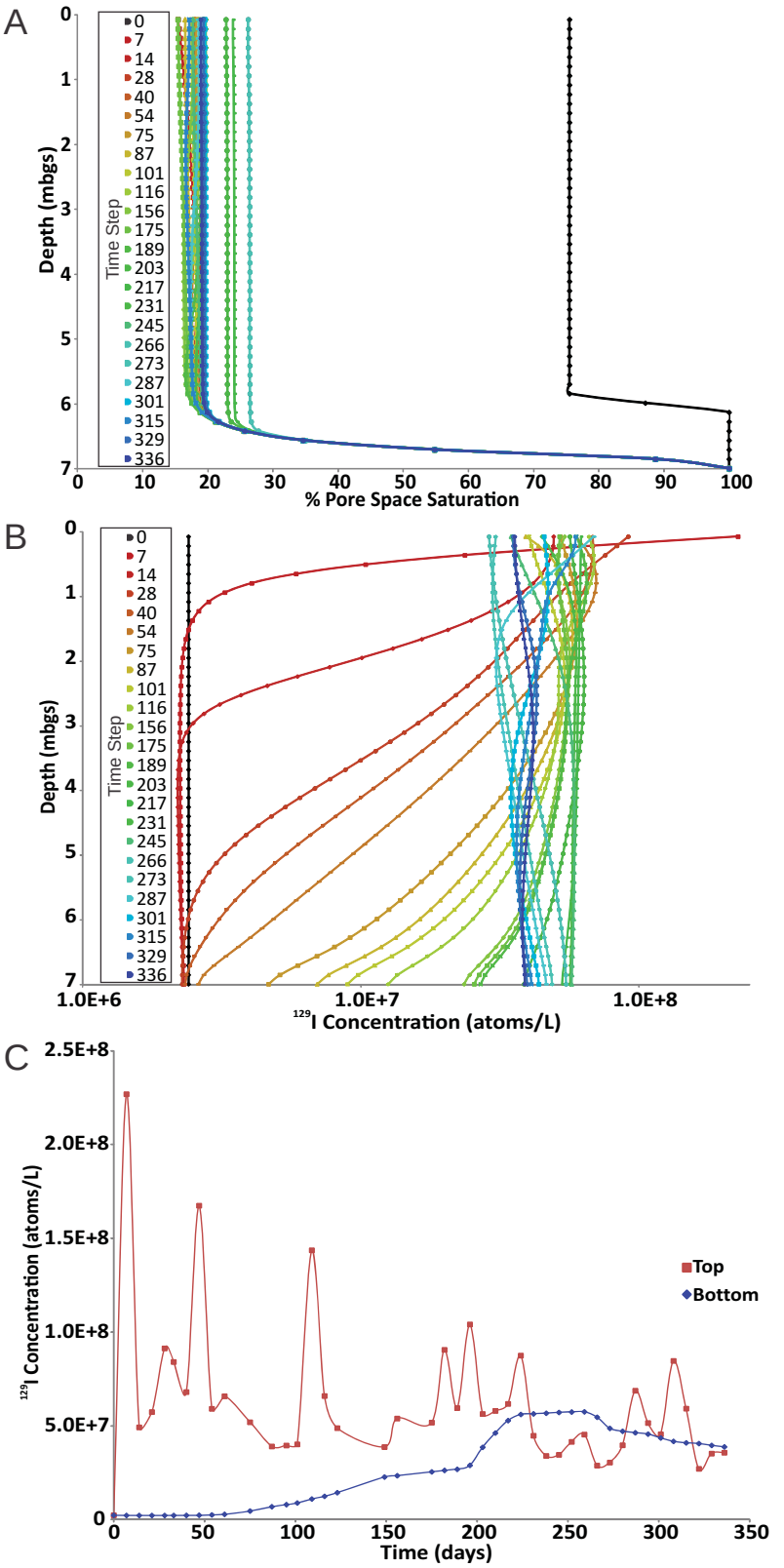

Figure 5. Modeling results in a vadose zone soil with 0 K_d for (a) the % pore saturation of the vadose zone with depth over time, (b) ^{129}I concentration with depth over time in which colors grade over time from red to blue, (c) ^{129}I concentration profile at the top of the section and the water table over time showing that some of the input variability which is recorded well at the top of the section is also preserved, although heavily attenuated, at the water table.

can preserve the changes in the input function and allow ^{129}I to behave conservatively, which agrees well with the observed pattern of ^{129}I concentration oscillation in ABB03 and PB20 samples. The preservation of input variability observed suggests that such a system is likely operating in the ASA vadose zone and that ^{129}I from the FDNA is being transported in such a flow path. Field observations of ASA stratigraphy support the existence of such beds (supporting information Figure S1).

3.2.4. Case II: Two Soil Scenario

Case II investigates the influence of a two layer vadose zone with different soil properties and differing K_d's on the transport of ^{129}I. In this scenario, a surface layer of sandy loam overlies the homogeneous sandy soil used in Case I. The K_d in the sandy soil below remained 0 while the sandy loam above had a K_d of 15 L/kg due to the presence of organic matter in such surface soils. Indeed, loss-on-ignition results for the upper 30 cm of the ASA soils have 3–9% organic matter. The sandy loam had a porosity of 0.49 and a K of 1.8 m/d, which was obtained from *Chesnaux and Allen* [2007]. The thickness of the sandy loam was 0.30 m. The simulation had a fluid error of 0.00% and a solute mass balance error of 5.84%.

Figure 6a shows that the surface sandy loam has a much higher saturation capacity than the coarser grained medium sand below, which will have a major effect on the transport of ^{129}I. Likewise, heterogeneity in the vertical distribution of the coarser facies in the field will establish preferential pathways for the transport of ^{129}I. There is field evidence for the existence of such conduits in the form of subvertical gravel cross-beds (supporting information Figure S1).

The depth profile of ^{129}I concentration seen in Figure 6b shows that in the first several recharge periods ^{129}I is almost fully retarded by the sandy loam, with breakthrough into the lower sand through to the water table occurring later in time.

Figure 6c shows the evolution of the ^{129}I concentration at the top of the section and the water table over time. The concentration of ^{129}I in the loam soil rises steadily throughout the simulation, through sorption. Only when equilibrium with the water is attained does ^{129}I start to pass through the upper soil, with the variability of the input damped. The ^{129}I concentration in the groundwater and the concentration throughout the depth profile appear to reach equilibrium by the end of the simulation. The initial increase in ^{129}I concentration at the water table appeared within ~95 days, with a maximum concentration of 10.5×10^6 atoms/L. This concentration is much closer to measured ^{129}I concentrations than those seen in Case I suggesting that a heterogeneous soil with various K_d's will lower the ^{129}I concentration in groundwater. The ^{129}I velocity in the sandy loam was 0.04 m/d, which is much lower than that modeled in Case I, with a much higher ^{129}I velocity in the medium sand (0.16 m/d). This latter value is nearly identical to the velocity in Case I.

Case II introduces heterogeneity into the vadose zone model in terms of both K_d and lithology, showing that this still allows ^{129}I transport to the water table with limited retardation. Case II however, fails to reproduce the variable ^{129}I concentration in groundwater arising from the variable input function. The smoothing effect, even with a low K_d, of the homogeneous sandy loam produces a cumulative increase in ^{129}I concentrations at the water table as opposed to the observed variability in ABB03 and PB20. Therefore, a model that incorporates a layer with a uniform K_d value cannot explain both the low ^{129}I concentrations in ASA wells and their temporal variability. Thus, a conceptual model for contaminant transport in the vadose zone of the ASA is one that incorporates preferential flow paths, with negligible sorption to provide conduits for the rapid infiltration of precipitation and ^{129}I, which preserve the variability of the input function.

3.2.5. Temporal Variability of ^{129}I and ^{129}I/^{127}I in Groundwater

The results of vadose zone modeling allow for a comparison between the timing of variations in modeled groundwater ^{129}I concentrations and the observed ^{129}I variation in samples from ABB03 and PB20. It is possible to use the breakthrough times found in modeling Cases I and II to evaluate if ^{129}I in washout from the FDNA could travel through the vadose zone, to the well screen within the time needed to produce the observed ^{129}I variability in groundwater samples. The ^{129}I peak in ABB03 occurred 0.93 years after Fukushima. The average ^{3}H/^{3}He groundwater age of ABB03 is 0.9 ± 0.5 years from the water table to well screen. Therefore, vadose zone travel time would have to be very rapid in order for ^{129}I from the FDNA to contribute to these elevated concentrations. Similarly, for PB20 the average ^{3}H/^{3}He groundwater age is 1.2 ± 0.5 years and the peak was observed at 1.35 years and is spread out over around 3 months (0.25 years).

Case I demonstrates the case for a rapid ^{129}I transport scenario, which we hypothesize represents an ideal preferential flow path that is the result of the heterogeneous lithology of the ASA soils. 0 K_d was applied

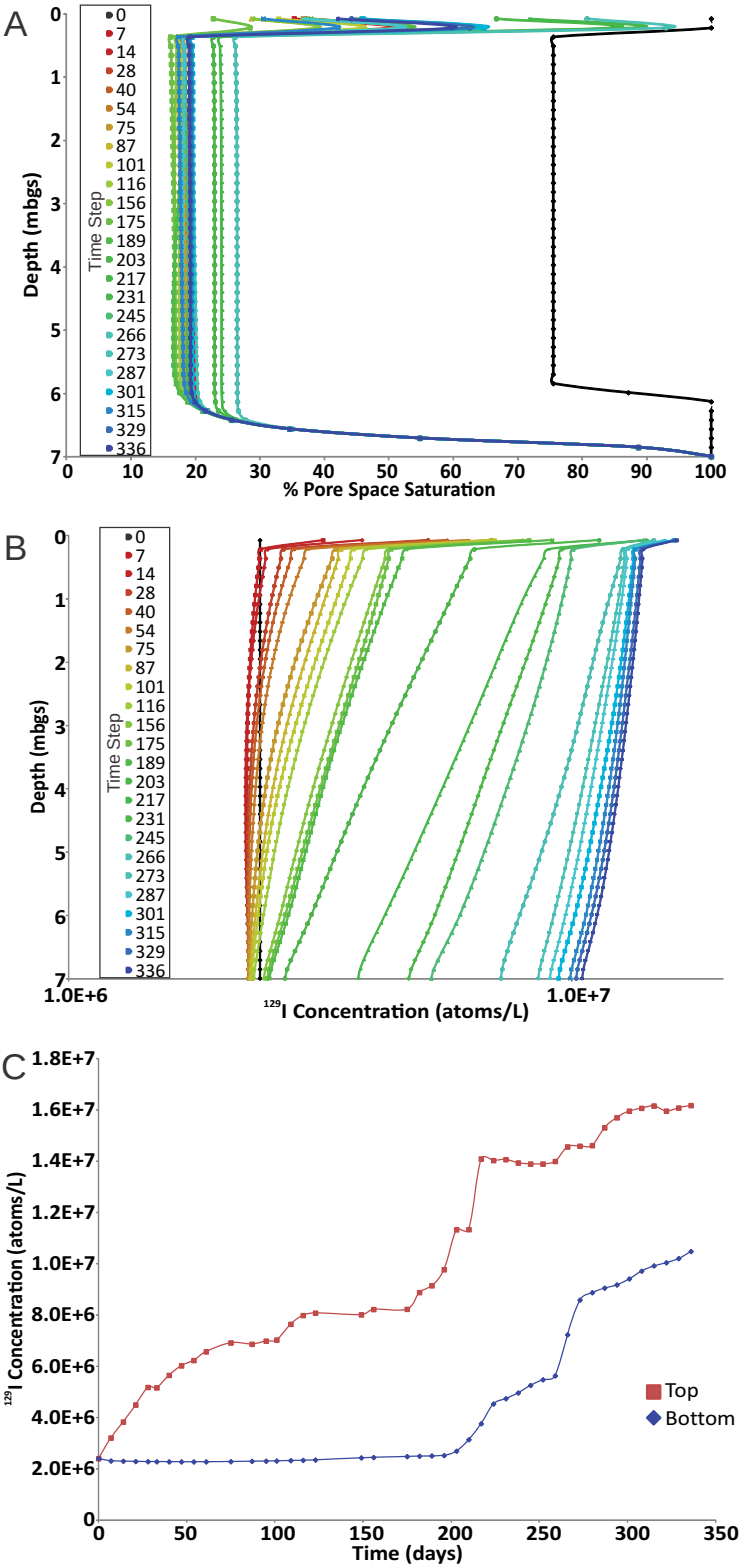

Figure 6. Modeling results in a vadose zone soil with a 30 cm surface soil with a K_d of 15 L/kg and an underlying sand with 0 K_d for (a) the % pore saturation of the vadose zone with depth over time, (b) ^{129}I concentration with depth over time in which colors grade over time from red to blue, (c) ^{129}I concentration profile at the water table and top of the section over time showing that the application of a high K_d layer near the ground surface accumulates ^{129}I leading to a similar trend at the water table which does not retain the variability measured as washout.

and the initial increase in ^{129}I concentrations observed after ~0.11 years and the peak was at ~0.71 years in the model results. These vadose zone travel times can then be added to the range of feasible groundwater ages for ABB03 and PB20 to get a range of model predictions for ^{129}I travel times from deposition on the ground surface to the well screen.

In ABB03, the range of modeled transport times is 0.5–1.5 years when using the time of the initial increase in ^{129}I concentrations as the vadose zone travel time. Using the travel time of the peak ^{129}I concentration in the model yields a range of 1.1–2.1 years. The agreement between these predicted times and the measured increases in ^{129}I concentration in ABB03 are excellent, although the timing of the initial increase is slightly better due to the smoothing that occurs to the ^{129}I peak as it traveled through the vadose zone. This is an indication that this model provides reasonable results in terms of transport times and that there is a high likelihood of rapid ^{129}I transport through the vadose zone in situations with almost no retardation. This agreement also suggests that the measured variability in ABB03 may be due to ^{129}I from the FDNA being rapidly transported to water table and that previous estimates for groundwater age in ABB03 are accurate. The modeled breakthrough times for the initial increase in PB20 ranged from 0.8 to 1.8 years and for the peak 1.4–2.4 years. These modeled ages are also in excellent agreement with observed variation in PB20 and strengthen the argument that ^{129}I from the FDNA could have been rapidly transported as both wells show measured ^{129}I increases at the same times as are predicted by modeling of vadose zone transport times summed with previously measured groundwater ages. We propose that this rapid transport of FDNA ^{129}I is possible if it was conducted via preferential flow paths that exist due to the heterogeneous stratigraphy of the ASA soils. These flow paths are capable of conducting ^{129}I with almost no retardation, similar to the situation modeled in Case 1. The only factor limiting ^{129}I transport was the degree of saturation of the soil as the well-drained nature of the vadose zone and the preferential flow paths retards ^{129}I transport. In the model cases, ^{129}I reached the water table very rapidly and has an effect on groundwater ^{129}I concentrations despite this limitation. ^{129}I transport via preferential flow paths can also explain the drop in ^{129}I concentrations between precipitation and groundwater as only a fraction of the ^{129}I is being transported rapidly, while a significant amount is likely attenuated by soils. The result is a scenario in which the degree of ^{129}I variability in the input is dampened in groundwater despite the rapid transport.

Case II included a surface soil with lower hydraulic conductivity and a K_d value of 15 L/kg. The initial increase in ^{129}I concentration at the water table in this model occurred after 0.26 years. The peak time for this scenario was reached at the end of the modeling time due to the cumulative increase in ^{129}I concentrations at the water table, which was not observed in actual groundwater measurements. Therefore, the timing of the initial increase provides the only data for estimating travel times in this scenario. In ABB03 the modeled range of ^{129}I breakthrough was 0.66–1.66 years and in PB20 it was 0.96–1.96 years. The modeled ages in both wells agree well with the ages for ^{129}I variability in both wells. This suggests that it is possible the vadose zone to have a small K_d value and still transport ^{129}I rapidly.

We propose a system in which a fraction of the ^{129}I in precipitation is conducted conservatively and rapidly, via preferential flow paths, through the vadose zone to the water table while the remainder is retarded and is ultimately homogenized with ^{129}I from other precipitation events and irrigation. This results in stable, low ^{129}I concentrations in groundwater, while some of the input variability is preserved due to the fraction of ^{129}I that is conservatively transported in the preferential flow paths. In the ASA homogenization is driven by a combination of soil-water partitioning and the low saturation of the soil, which leads to a higher degree of retardation. The ^{129}I travel times modeled here may also apply to other contaminants released on the ground surface of the ASA.

The final phase of ^{129}I transport is the saturated zone movement from the water table to the well screen where it is sampled. During groundwater transport, lateral, longitudinal and vertical dispersion or mixing effects will likely result in lowering the ^{129}I concentration in groundwater below that modeled at the water table to the ^{129}I concentrations that were actually measured in samples from ABB03 and PB20. However, in shallow portions of the aquifer it has been concluded that flow is predominantly subvertical and that mixing will be more limited due to relatively short transport distances [*Wassenaar et al.*, 2006; *Chesnaux et al.*, 2012]. Ultimately, some dilution of the event-based pulse of the FDNA ^{129}I is occurring, but it is considered minimal due to the shallow depths of the well screens and the rapid vertical flow of water in the shallow portions of the ASA.

4. Summary and Conclusions

The atmospheric transport of ^{129}I from the Fukushima-Daichii Nuclear Accident and its deposition via precipitation has been quantified for a year following the accident using weekly precipitation sampling. The transport of ^{129}I has also been traced into local groundwater to elucidate the long term fate of the ^{129}I. The data show that FDNA ^{129}I was rapidly transported to the west coast of North America and was first detected on the week of 17 March 2011 within 6–8 days of the accident. This pulse is corroborated by samples taken from three sampling locations: Vancouver, Saturna Island, and the NADP site WA-19. The peak magnitude of the FDNA pulse, 211×10^6 atoms ^{129}I/L, was approximately 7 times above pre-accident background of 31×10^6 atoms/L. However, ^{129}I concentrations returned to background levels within a few days suggesting relatively little mixing of ^{129}I between air masses during trans-Pacific transport. Several precipitation events with ^{129}I concentrations substantially higher than background were also observed throughout the year including one in July with a concentration even higher than that measured directly following the FDNA. These peaks occurred after most atmospheric radionuclide monitoring for FDNA fission products has ceased and their cause is likely due to a combination of natural processes such as resuspension from the ground surface, ocean volatilization and atmospheric concentration due to drought periods as well as releases from nuclear fuel reprocessing.

The peak ^{129}I mass flux was observed immediately following the FDNA and in the same sampling period that contained the peak ^{129}I concentration. The ^{129}I concentration is the principle factor determining washout. The correlation coefficient between the ^{129}I concentration and washout is greater than that for the precipitation quantity.

Groundwater ^{129}I concentrations in two nearby wells showed minor anomalies over the sampling period which could be due to rapid infiltration of the FDNA atmospheric ^{129}I signal. Vadose zone modeling shows that it was possible for a component of the ^{129}I deposited by the FDNA to be conducted rapidly from the ground surface to the water table along preferential flow paths with little retardation such that anomalies within the input signal can be observed at the water table. The balance of the input ^{129}I, in contrast, traveled through the upper soil with a K_d value of ~15 L/kg where variable input concentrations were attenuated.

We conclude that it is possible that a fraction of ^{129}I from the FDNA is transported conservatively in this aquifer via preferential flow paths to the water table while the remaining ^{129}I in the system interacts with soil and its transport is retarded within the vadose zone. The result is that attenuated ^{129}I anomalies of atmospheric origin can be observed in the groundwater. Further, the modeled lag times of these attenuated atmospheric anomalies are consistent with ^{3}H/^{3}He groundwater ages previously measured in two separate wells. This finding helps constrain contaminant and/or tracer transport from the ground surface to the water table in the ASA.

This paper provides, for the first time, insight into the transport of ^{129}I from an atmospheric release and its fate during wet deposition and recharge to groundwater. While ^{129}I is largely retained on organics in the soil of the upper vadose zone the long term fate of ^{129}I from the FDNA includes recharge into the Abbotsford-Sumas aquifer groundwaters. Continuing work on the fate of ^{129}I and its transport should address the influence of local redox conditions in detail and the inorganic and organic speciation of ^{129}I and ^{127}I in precipitation, the vadose zone, and groundwater.

Acknowledgments
The authors would like to thank Rick Healy for his assistance with using VS2DTI and Romain Chesnaux for his advice concerning modeling the vadose zone of the Abbotsford-Sumas Aquifer. Thanks are also owed to Greg Wetherbee of the USGS and Christopher Lehmann of National Atmospheric Deposition Program for providing precipitation samples. The authors are also grateful for the map making of Tommy Diep from Environment Canada. Data may be found in the supporting information or by contacting MNH.

References

Aldahan, A., V. Alfimov, and G. Possnert (2007), ^{129}I anthropogenic budget: Major sources and sinks, *Appl. Geochem.*, *22*(3), 606–618, doi:10.1016/j.apgeochem.2006.12.006.

Aldahan, A., S. Persson, G. Possnert, and X. L. Hou (2009), Distribution of ^{127}I and ^{129}I in precipitation at high European latitudes, *Geophys. Res. Lett.*, *36*, L11805, doi:10.1029/2009GL037363.

Alvarado-Quiroz, N. G., T. G. Kotzer, G. M. Milton, I. D. Clark, and D. Bottomley (2002), Partitioning of ^{127}I and ^{129}I in an unconfined glaciofluvial aquifer on the Canadian shield, *Radiochim. Acta*, *90*(8), 469–478.

Baker, A. R., C. Tunnicliffe, and T. D. Jickells (2001), Iodine speciation and deposition fluxes from the marine atmosphere, *J. Geophys. Res.*, *106*, 28,743–28,749.

Bamba, S., K. E. Yamaguchi, and H. Amano (2014), Determination of ^{129}I/^{127}I in environmental water before and after the 2011 Fukushima Daiichi nuclear power plant accident with a solid extraction disk, *J. Radioanal. Nucl. Chem.*, *301*(1), 75–80, doi:10.1007/s10967-014-3055-8.

Bartholomay, R. C. (2013), Iodine-129 in the Eastern Snake River Plain Aquifer at and near the Idaho National Laboratory, Idaho, 2010–12, *U.S. Geol. Surv. Sci. Invest. Rep., 2013-5195*, pp. 1–22.

Bikit, I., D. Mrda, N. Todorovic, J. Nikolov, M. Krmar, M. Veskovic, J. Slivka, J. Hansman, S. Forkapic, and N. Jovancevic (2012), Airborne radioiodine in northern Serbia from Fukushima, *J. Environ. Radioact.*, *114*, 89–93, doi:10.1016/j.jenvrad.2012.01.020.

Brauer, F. P., and H. G. J. Rieck (1973), ^{129}I, ^{60}Co, ^{106}Ru measurements on water samples from the Hanford Project Environs, *Rep. BNWL-SA-4478*, Pacific Northwest National Laboratories, Richland, Wash.

Chesnaux, R., and D. M. Allen (2007), Simulating nitrate leaching profiles in a highly permeable vadose zone, *Environ. Model. Assess.*, *13*(4), 527–539, doi:10.1007/s10666-007-9116-4.
Chesnaux, R., D. M. Allen, and G. Graham (2007), Assessment of the impact of nutrient management practices on nitrate contamination in the Abbotsford-Sumas aquifer, *Environ. Sci. Technol.*, *41*(21), 7229–7234.
Chesnaux, R., D. M. Allen, and M. W. M. Simpson (2012), Comparing isotopic groundwater age measurements with simulated groundwater ages: Example of the Abbotsford-Sumas Aquifer (USA and Canada) and application, *Water Environ. J.*, *26*(1), 30–37, doi:10.1111/j.1747-6593.2011.00260.x.
Cox, S. E., and S. C. Kahle (1999), Hydrogeology, ground-water quality, and source of nitrate in lowland glacial aquifers of Whatcom County, Washington and British Columbia, Canada, *Water Invest. Rep. 98–4195*, U.S. Geol. Survey Tacoma, Wash.
Draxler, R. R., and G. D. Rolph (2013), Real-time Environmental Applications and Display sYstem (READY). NOAA Air Resour. Lab., College Park, Md. [Available at http://www.ready.noaa.gov.]
Evrard, O., P. Van Beek, D. Gateuille, V. Pont, I. Lefèvre, B. Lansard, and P. Bonté (2012), Evidence of the radioactive fallout in France due to the Fukushima nuclear accident, *J. Environ. Radioact.*, *114*, 1–7, doi:10.1016/j.jenvrad.2012.01.024.
Fabryka-Martin, J., D. O. Whittemore, S. N. Davis, P. W. Kubik, and P. Sharma (1991), Geochemistry of halogens in the Milk River aquifer, Alberta, Canada, *Appl. Geochem.*, *6*(1), 447–464.
Farmwest (1998), *Farmwest-Penman Monteith Equation*, Pacific Field Corn Association, pp. 1–12. [Available at http://www.farmwest.com/climate/et.]
Freeze, R. A., and J. A. Cherry (1979), *Groundwater*, 1st ed., Prentice Hall, Englewood Cliffs, N. J.
Fuge, R., and C. Johnson (1986), The geochemistry of iodine—A review, *Environ. Geochem. Health*, *8*(2), 31–54.
Fukui, M., Y. Fujikawa, and N. Satta (1996), Factors affecting interaction of radioiodide and iodate species with soil, *J. Environ. Radioact.*, *31*(2), 199–216, doi:10.1016/0265-931X(95)00039-D.
Gilfedder, B. S., M. Petri, and H. Biester (2007), Iodine and bromine speciation in snow and the effect of orographically induced precipitation, *Atmos. Chem. Phys.*, *7*(10), 2661–2669, doi:10.5194/acp-7-2661-2007.
Gilfedder, B. S., S. C. Lai, M. Petri, H. Biester, and T. Hoffmann (2008), Iodine speciation in rain, snow and aerosols, *Atmos. Chem. Phys.*, *8*, 6069–6084.
Gómez-Guzmán, J. M., S. M. Enamorado-Báez, A. R. Pinto-Gómez, J. M. Abril-Hernández, J. M. López-Gutiérrez, and M. García-León (2012), Anthropogenic ^{129}I concentration and ^{129}I/^{127}I ratio in rainwater from Seville (Spain) in the period 2005–2008 as affected by airborne releases from Sellafield and La Hague facilities, *Atmos. Environ.*, *56*, 26–32, doi:10.1016/j.atmosenv.2012.03.075.
Graham, G., D. M. Allen, and B. Finkbeiner (2014), Climate controls on nitrate concentration variability in the Abbotsford-Sumas aquifer, British Columbia, Canada, *Environ. Earth Sci.*, *73*, 2895–2907, doi:10.1007/s12665-014-3072-5.
Health Canada (2014), Radiation monitoring data and the nuclear emergency in Japan. [Available at http://www.hc-sc.gc.ca/hc-ps/ed-ud/respond/nuclea/data-donnees-eng.php.]
Healy, R. W. (1990), Simulation of solute transport in variably saturated porous media with supplemetal information on modifications to the U.S. Geological Survey's Computer Program VS2D, *U.S. Geol. Surv. Water Resour. Invest. Rep., 90-4025*, pp. 1–125.
Herod, M. N., I. D. Clark, W. E. Kieser, S. Agosta, and X.-L. Zhao (2013), ^{129}I dispersion and sources in Northwest Canada, *Nucl. Instrum. Methods Phys. Res., Sect. B*, *294*, 552–558, doi:10.1016/j.nimb.2012.06.018.
Hii, B., H. Liebscher, M. Mazalek, T. Tuominen, A. S. Division, E. C. Branch, E. Canada, and Y. Region (1999), *Ground Water Quality and Flow Rates in the Abbotsford Aquifer, British Columbia*, Aquatic and Atmospheric Science Division Environmental Conservation Branch Environment Canada, Pacific and Yukon Region, Vancouver, B. C.
Hou, X., V. Hansen, A. Aldahan, G. Possnert, O. C. Lind, and G. Lujaniene (2009), A review on speciation of iodine-129 in the environmental and biological samples, *Anal. Chim. Acta*, *632*(2), 181–196, doi:10.1016/j.aca.2008.11.013.
Hu, Q., P. Zhao, J. E. Moran, and J. C. Seaman (2005), Sorption and transport of iodine species in sediments from the Savannah River and Hanford Sites, *J. Contam. Hydrol.*, *78*(3), 185–205, doi:10.1016/j.jconhyd.2005.05.007.
Hu, Q. H., J. E. Moran, and J. Y. Gan (2012), Sorption, degradation, and transport of methyl iodide and other iodine species in geologic media, *Appl. Geochem.*, *27*(3), 774–781, doi:10.1016/j.apgeochem.2011.12.022.
Jabbar, T., G. Wallner, and P. Steier (2013), A review on (129)I analysis in air, *J. Environ. Radioact.*, *126C*, 45–54, doi:10.1016/j.jenvrad.2013.07.013.
Landis, J. D., N. T. Hamm, C. E. Renshaw, W. B. Dade, F. J. Magilligan, and J. D. Gartner (2012), Surficial redistribution of fallout ^{131}iodine in a small temperate catchment, *Proc. Natl. Acad. Sci. U. S. A.*, *109*(11), 4064–4069, doi:10.1073/pnas.1118665109.
Lapala, E. G., R. W. Healy, and E. Weeks (1987), Documentation of the comupter program VS2D to solve the equations of fluid flow in variably saturated porous media, *U.S. Geol. Surv. Water Resour. Invest. Rep., 83-4099*, pp. 1–184.
Lehto, J., T. Räty, X. Hou, J. Paatero, A. Aldahan, G. Possnert, J. Flinkman, and H. Kankaanpää (2012), Speciation of ^{129}I in sea, lake and rain waters, *Sci. Total Environ.*, *419*, 60–67, doi:10.1016/j.scitotenv.2011.12.061.
Leon, J. D., D. A. Jaffe, J. Kaspar, A. Knecht, M. L. Miller, R. G. H. Robertson, and A. G. Schubert (2011), Arrival time and magnitude of airborne fission products from the Fukushima, Japan, reactor incident as measured in Seattle, WA, USA, *J. Environ. Radioact.*, *102*(11), 1032–1038.
López-Gutiérrez, J. M., M. García-León, C. Schnabel, M. Suter, H. A. Synal, and S. Szidat (2001), Wet and dry deposition of ^{129}I in Seville (Spain) measured by accelerator mass spectrometry, *J. Environ. Radioact.*, *55*(3), 269–282.
Macmullin, S., G. K. Giovanetti, M. P. Green, R. Henning, R. Holmes, K. Vorren, and J. F. Wilkerson (2012), Measurement of airborne fission products in Chapel Hill, NC, USA from the Fukushima Daiichi reactor accident, *J. Environ. Radioact.*, *112*, 165–170, doi:10.1016/j.jenvrad.2012.01.026.
Melgunov, M. S., N. P. Pokhilenko, V. D. Strakhovenko, F. V. Sukhorukov, and A. V. Chuguevskii (2012), Fallout traces of the Fukushima NPP accident in southern West Siberia (Novosibirsk, Russia), *Environ. Sci. Pollut. Res. Int.*, *19*(4), 1323–1325, doi:10.1007/s11356-011-0659-1.
Mitchell, R. J., R. S. Babcock, S. Gelinas, L. Nanus, and D. E. Stasney (2003), Nitrate distributions and source identification in the Abbotsford-Sumas Aquifer, Northwestern Washington State, *J. Environ. Qual.*, *32*, 789–800.
Miyake, Y., H. Matsuzaki, T. Fujiwara, T. Saito, T. Yamagata, M. Honda, and Y. Muramatsu (2012), Isotopic ratio of radioactive iodine (^{129}I/^{131}I) released from Fukushima Daiichi NPP accident Fukushima, *Geochem. J.*, *46*, 327–333.
Moran, J. E., S. D. Oktay, P. H. Santschi, and D. R. Schink (1999), Atmospheric dispersal of 129 Iodine from nuclear fuel reprocessing facilities, *Environ. Sci. Technol.*, *33*(15), 2536–2542.
Muramatsu, Y., Y. Uchida, P. Sriyotha, and K. Sriyotha (1990), Some considerations on the sorption and desorption phenomena of iodide and iodate on soil, *Water Air Soil Pollut.*, *49*, 125–138.

Muramatsu, Y., H. Matsuzaki, C. Toyama, and T. Ohno (2015), Analysis of ^{129}I in the soils of Fukushima Prefecture: Preliminary reconstruction of ^{131}I deposition related to the accident at Fukushima Daiichi Nuclear Power Plant (FDNPP), *J. Environ. Radioact.*, *134*, 344–350, doi:10.1016/j.jenvrad.2014.05.007.

Paul, M., D. Fink, G. Hollos, A. Kaufman, W. Kutschera, and M. Magaritz (1987), Measurement of ^{129}I concentrations in the environment after the Chernobyl reactor accident, *Nucl. Instrum. Methods Phys. Res., Sect. B*, *29*(1–2), 341–345, doi:10.1016/0168-583X(87)90262-X.

Persson, S., A. Aldahan, G. Possnert, V. Alfimov, and X. Hou (2007), ^{129}I variability in precipitation over Europe, *Nucl. Instrum. Methods Phys. Res., Sect. B*, *259*(1), 508–512, doi:10.1016/j.nimb.2007.01.193.

Piñero García, F., and M. A. Ferro García (2012), Traces of fission products in southeast Spain after the Fukushima nuclear accident, *J. Environ. Radioact.*, *114*, 146–151, doi:10.1016/j.jenvrad.2012.01.011.

Reithmeier, H., V. Lazarev, W. Rühm, T. M. Schwikowski, H. W. Gäggeler, and E. Nolte (2006), Estimate of European ^{129}I releases supported by ^{129}I analysis in an Alpine ice core, *Environ. Sci. Technol.*, *40*(19), 5891–5896.

Schwehr, K. A., P. H. Santschi, J. E. Moran, and D. Elmore (2005), Near-conservative behavior of ^{129}I in the Orange County aquifer system, California, *Appl. Geochem.*, *20*(8), 1461–1472, doi:10.1016/j.apgeochem.2005.02.003.

Schwehr, K. A., P. H. Santschi, D. J. Kaplan, C. M. Yeager, and R. Brinkmeyer (2009), Organo-iodine formation in soils and aquifer sediments at ambient concentrations, *Environ. Sci. Technol.*, *43*(19), 7258–7264.

Scibek, J., and D. Allen (2006), Comparing modelled responses of two high-permeability, unconfined aquifers to predicted climate change, *Global Planet. Change*, *50*(1–2), 50–62, doi:10.1016/j.gloplacha.2005.10.002.

Sheppard, M. I., D. H. Thibault, J. McMurry, and E. A. Smith (1995), Factors affecting the soil sorption of iodine, *Water Air Soil Pollut.*, *83*, 51–67.

Sheppard, M. I., J. L. Hawkins, and P. A. Smith (1996), Soil processes and chemical transport: Linearity of iodine sorption and sorption capacities for seven soils, *J. Environ. Qual.*, *25*, 1261–1267.

Sheppard, S. C., and M. Herod (2012), Variation in background concentrations and specific activities of ^{36}Cl, ^{129}I and U/Th-series radionuclides in surface waters, *J. Environ. Radioact.*, *106*, 27–34, doi:10.1016/j.jenvrad.2011.10.015.

Söderlund, M., M. Lusa, J. Lehto, and M. Hakanen (2011), *POSIVA Working Report 2001-04: Sorption of Iodine, Chlorine, Technetium and Cesium in Soil*, POSIVA.

Steinhauser, G. (2014), Fukushima's forgotten radionuclides: A review of the understudied radioactive emissions, *Environ. Sci. Technol.*, *48*(9), 4649–4663, doi:10.1021/es405654c.

Tokyo Electric Power Company (2012), *Estimation of Radioactive Material Released to the Atmosphere During the Fukushima Daiichi NPS Accident*.

van Genuchten, M. T. (1980), A closed-form equation for predicting the hydraulic conductivity of unsaturated soils, *Soil Sci. Soc. Am. J.*, *44*(5), 892, doi:10.2136/sssaj1980.03615995004400050002x.

Wassenaar, L. I. (1995), Evaluation of the origin and fate of nitrate in the Abbotsford Aquifer using the isotopes of 15N and 180 in NO^{3-}, *Appl. Geochem.*, *10*, 391–405.

Wassenaar, L. I., M. J. Hendry, and N. Harrington (2006), Decadal geochemical and isotopic trends for nitrate in a transboundary aquifer and implications for agricultural beneficial management practices, *Environ. Sci. Technol.*, *40*(15), 4626–4632.

Wetherbee, G. A., D. A. Gay, T. M. Debey, C. M. B. Lehmann, and M. A. Nilles (2012), Wet Deposition of Fission-Product Isotopes to North America from the Fukushima Dai-ichi Incident, March 2011, *Environ. Sci. Technol.*, *46*(5), 2574–2582.

Xu, C., et al. (2011), Is soil natural organic matter a sink or source for mobile radioiodine (^{129}I) at the Savannah River Site, *Geochim. Cosmochim. Acta*, *75*(19), 5716–5735, doi:10.1016/j.gca.2011.07.011.

Xu, S., S. P. H. T. Freeman, X. Hou, A. Watanabe, K. Yamaguchi, and L. Zhang (2013), Iodine isotopes in precipitation: Temporal responses to ^{129}I emissions from the Fukushima nuclear accident, *Environ. Sci. Technol.*, *47*(19), 10,851–10,859, doi:10.1021/es401527q.

Zebarth, B. J., M. C. Ryan, G. Graham, T. A. Forge, and D. Neilsen (2015), Groundwater monitoring to support development of BMPs for groundwater protection: The Abbotsford-Sumas Aquifer case study, *Ground Water Monit. Rem.*, *35*(1), 82–96, doi:10.1111/gwmr.12092.

Zhang, S., et al. (2011), Concentration-dependent mobility, retardation, and speciation of iodine in surface sediment from the Savannah River Site, *Environ. Sci. Technol.*, *45*(13), 5543–5549, doi:10.1021/es1040442.